

# Flow Characteristics of the Sound Pressure level and its Prediction for a Low Pressure Axial Flow Fan

by

Yoshio KODAMA\*, Hidechito HAYASHI\*, Kiyohiro TANAKA\*  
Hidehiko KAWABE\* and Masato KURISU\*

## 1. Introduction

The noise generated from a fan changes in the flow rate<sup>(1)~(3)</sup>. That is, the sound pressure level is minimum near the maximum point of a fan efficiency and in this flow region the fan noise consists of the turbulent noise and rotating noise<sup>(4)</sup>. The latter can be decreased by the combination of the number of rotor blades and stator vanes or the arrangement of them to be ignored<sup>(5)(6)</sup>. Therefore, the turbulent noise is main at the design point. The authors have investigated about the effects of each factor on the fan noise in detailed and proposed the flow model to introduce formulae considered these factors, and we made clearly it to be valid comparing those with experiments<sup>(7)</sup>.

When the flow rate is decreased, the fan noise increases gradually and becomes maximum at some flow rate. In this flow rate region, it is seen in many cases that the discrete frequency noise generated with the another source. This noise generated by the resonance with the turbulence of the wake and fan system. But it can be decreased to the turbulent noise level by making the tip clearance small<sup>(8)</sup>. Therefore, in low flow rate region the turbulent noise is also important. The relation between the turbulent noise level and the flow rate was pointed out by other investigators<sup>(9)</sup>, but they have not given the quantitative explanation for such flow characteristics of the sound pressure level.

In this paper, we discussed the relation between the turbulent noise and the flow condition around rotor blades; the wake widths and relative velocities. Then we predict the sound pressure level in each flow condition theoretically.

## 2. Experimental Apparatus and Procedure

Figure 1 shows the schematic diagram of the experimental apparatus. The total length of the duct is about 14m. An inlet nozzle is installed at the inlet and a conical damper is provided at the exit to adjust the flow rate. A test fan is connected with a diffuser. i. e., a connecting duct to a circular of 624mm I. D., which

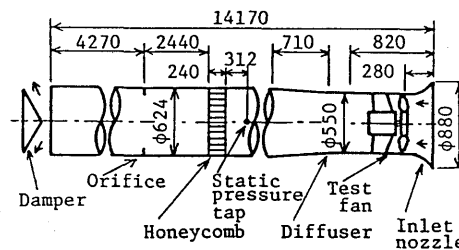


Fig. 1 Schematic diagram of experimental apparatus.

is equipped with a honeycomb and an orifice flow meter.

The impeller used in this experiment are shown in figure 2. This is the Clark Y-blade impeller of 530mm in diameter; it is referred to NCI in the following. The rotational frequency of NCI is about 1760rpm. As the casing diameter is 531.6mm, the tip clearance  $\bar{s}$  averaged circumferentially is 0.8mm.

The turbulent noise in this experiment has an intensity distribution of dipole type and its source axis is coincide with the rotor axis. Therefore, the sound pressure level was measured by a condenser microphone on the rotor axis at 1.5m upstream, and the output signals from a Brüel & Kjaer sound level meter were analyzed by a narrow band frequency analyzer with the ratio of band width to center frequency being 2.5%. The spectral density distribution was recorded with a high speed level recorder. The flows around rotor blades were measured by a five holes sphere type pitot tube and a hot-wire anemometer. Further, the output signals from the anemometer were analyzed by a FFT-analyzer and the spectral distribution averaged 200 times with adjusting the shaft rotation was recorded with a X-Y recorder. These flow measurements were carried out at the 41mm upstream section of the rotor blade leading edge ( $Z=41\text{mm}$ ) and 30mm downstream of the trailing edge ( $Z=-30\text{mm}$ ). At each section 10 points are measured and the space of each point is about 2~20mm.

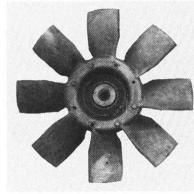


Fig. 2 Impeller used in this experiment (NCI-fan).

### 3. Theoretical formulae of turbulent noise

The turbulent noise from a single rotor fan is mainly caused by the vortex shedding from the blade trailing edges when the upstream flow condition is effectively smooth. The authors introduced the following formula to predict that noise

$$E = \pi B \rho \int_{\text{span}} DW^6 dR / 2400 a_0^3 \quad (1)$$

where  $E$  is the acoustic power,  $B$  the number of rotor blade,  $\rho$  the air density,  $D$  the wake width,  $W$  the relative velocity at rotor inlet,  $R$  the radial distance,  $a_0$  the sonic velocity.

Authors proposed a method to estimate  $D$  and it was shown that its results well agreed with experimental values at the design point<sup>(7)</sup>. In this report, we applied the equation (1) in the low flow rate region and explained the characteristics of sound pressure level shown in figure 3. The relation between the acoustic power and sound pressure level is given by following equation

$$\text{SPL} = 10 \log_{10} (3 \rho a_0 E / 8 \pi r^2 p_0^2) \quad (2)$$

where  $p_0$  is the reference sound pressure level ( $= 2 * 10^{-5} \text{ Pa}$ ),  $r$  the distance between an observer (microphone) and a noise source which is assumed to be at the center of the cross-section of the nozzle inlet.

## 4. Experimental Results and Discussion

4.1 Performance characteristics The characteristics of the tested fan is shown in figure 3. In the figure  $\psi$ ,  $\lambda$ ,  $\phi$  and  $\eta$  are the total pressure coefficient, the flow coefficient, the input power coefficient

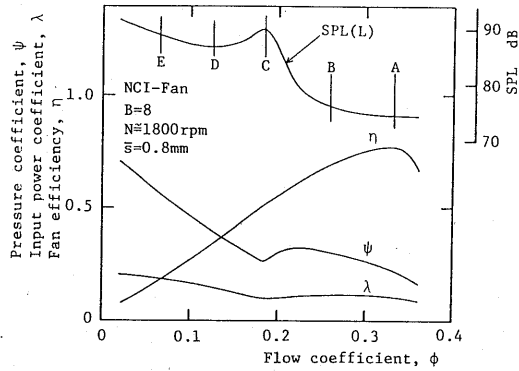


Fig. 3 Characteristic curve for NCI-fan.

to the electric motor and the combined efficiency of the motor and the fan respectively. And they are expressed as follows

$$\phi = 4Q/\pi(1-\nu^2)D_R^2 U_T, \quad \psi = 2P_T/\rho U_T^2 \tag{3}$$

$$\lambda = 816L/\pi\rho(1-\nu^2)D_R^2 U_T^3, \quad \eta = \phi\psi/\lambda$$

where  $Q$ ,  $\nu$ ,  $D_R$ ,  $U_T$ ,  $P_T$  and  $L$  are the flow rate, hub/tip ratio, impeller diameter, rotor tip speed, total pressure and the input power to the electric motor.

In this figure, SPL(L) is the sound pressure level measured with the sound level meter in L-characteristics. Figure 3 shows that the value of SPL(L) is the lowest at  $\eta_{max}$ -point ( $\phi=0.333$ ) as referred to SPL  $\eta_{max}$  and increases barely with reducing the flow rate until  $\phi$  is about 0.24. But under  $\phi=0.24$  SPL(L) abruptly increases and becomes maximum at about  $\phi=0.17$  where pressure coefficient becomes minimum.

4.2 Flow characteristics around rotor blades We investigate the relation between turbulent noise and the flow condition around rotor blades at five flow rate points (A-E) shown in figure 3. A is the maximum point of the fan efficiency ( $\phi=0.333$ ), B is the point where the sound pressure level is beginning to increase abruptly which is referred to SPL<sub>SI</sub>-point ( $\phi=0.25$ ), C is the point where the sound pressure level is maximum which is referred to SPL<sub>max</sub>-point ( $\phi=0.17$ ), D is the point where sound pressure level is minimum which is referred to SPL<sub>min</sub>-point ( $\phi=0.10$ ) and E is near the cut-off point ( $\phi=0.07$ ).

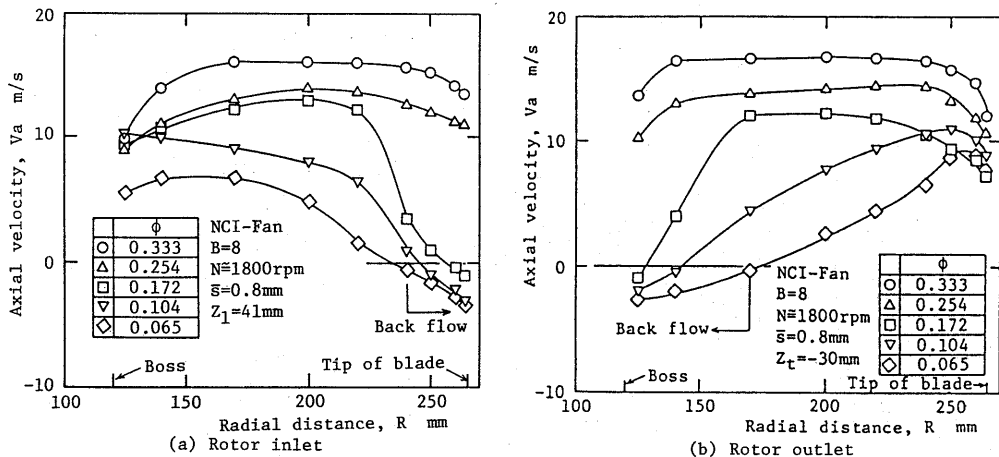


Fig. 4 Comparison of axial velocity.

Figure 4 (a) and (b) show the axial velocity distribution at rotor inlet ( $Z=41\text{mm}$ ) and outlet ( $Z=-30\text{mm}$ ). In the  $\text{SPL}_{\eta_{\max}}$ -point and  $\text{SPL}_{\text{SI}}$ -point, the velocity distributions are flat except the vicinity of boss and blade tip. These distributions decrease with decreasing flow rate over the whole radial positions. The degree of these decrease is large toward the tip at the rotor inlet, but toward the boss at the rotor outlet. In the flow rate region smaller than 0.172, back flow arises eventually. In the case of  $\phi=0.065$  (symbols  $\diamond$ ), the back flow region comes up to 1/3 blade height.

To check the flow conditions at each flow rate the incidence and deviation angles are shown in figure 5 and 6 respectively. The incidence angles are large where the sound pressure level is high. And the deviation angles are large near the blade tip when sound pressure level is higher. At  $\eta_{\max}$ -point the deviation angles are small over the whole radial locations, and these angles increase toward boss at the low flow rate and the degree of increase is remarkable in  $\phi \leq 0.172$ .

Figure 7 shows the relative velocity distribution at the rotor inlet for each flow rate. There is no difference in these distributions between at the  $\eta_{\max}$ -point where the sound pressure level is the lowest (symbols  $\circ$ ) and at the  $\text{SPL}_{\text{SI}}$ -point (symbols  $\triangle$ ). But at the  $\text{SPL}_{\max}$ -point (symbols  $\square$ ) the relative velocity is smaller than the formers caused by the back flow near the blade tip. From the above, we propose the flow configuration in figure 8 at the back flow condition.

4.3 Velocity fluctuation and wake width at the outlet section of rotor Figure 9 (a) and (d) show the trace of the velocity fluctuations for the radial position  $R=262\text{mm}$  and  $200\text{mm}$  (near the position of the root mean square) at each flow rate. It is difficult to distinguish clearly the main flow from the wake at all flow rate except  $\phi=0.333$  and  $0.254$ . Therefore, we average the traces in the amount of 200 revolutions with FFT-analyzer. If we do such management, the eight cleared peaks for eight blades can be get as

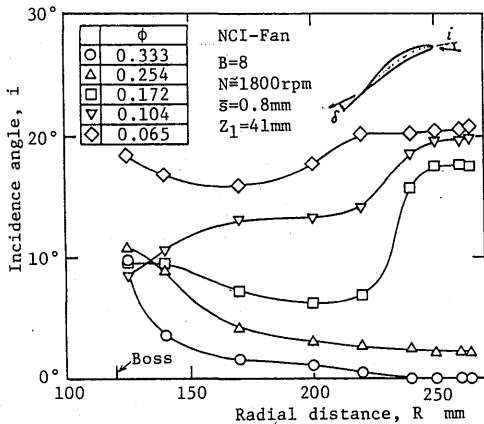


Fig. 5 Comparison of incidence angle.

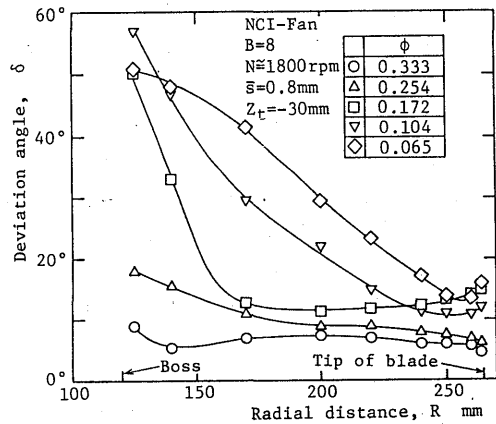


Fig. 6 Comparison of deviation angle.

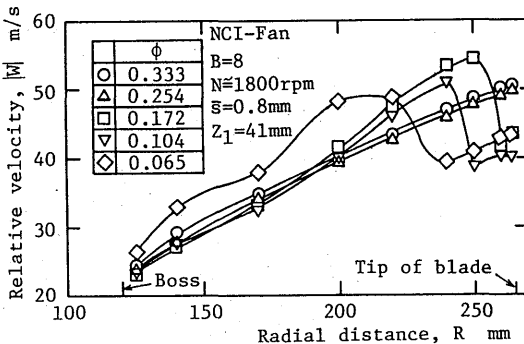


Fig. 7 Comparison of relative velocity.

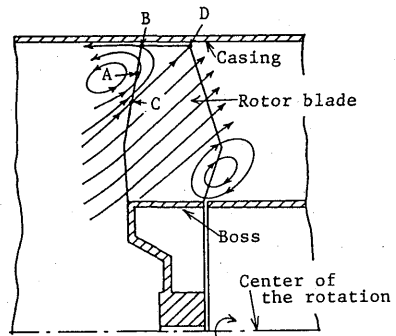


Fig. 8 Schematic diagram of flow pattern at low flow rate region.

shown figure 9 (a) and (b). It is difficult to define wake width from these velocity traces, but in this study, we proposed to adopt the width at half depth of wake ( $Da$ ) as the wake width in figure 9(a). According to this definition, the change of the sound pressure level due to flow rate well agrees with the change of the wake wake width at the blade tip ( $R=262\text{mm}$ ) and so we mentioned it in the next section.

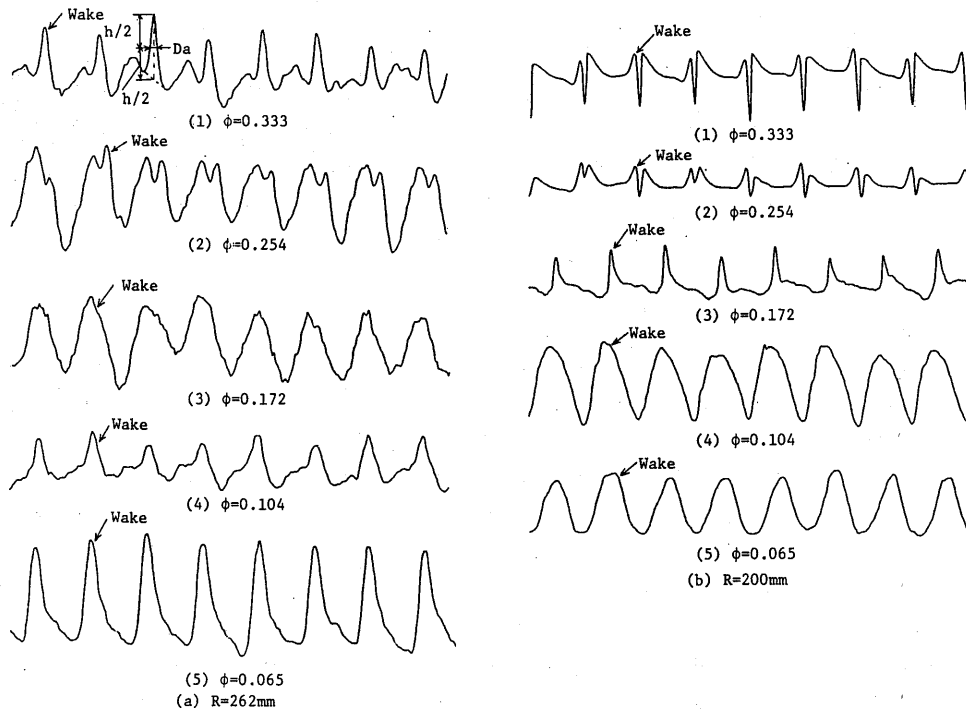


Fig. 9 Velocity fluctuation in the wake.  
(NCI-fan,  $\bar{s}=0.8\text{mm}$ )

4.4 Prediction of sound pressure level As the wake width  $D$  included equation (1) is in the relative coordinate system, we estimate  $D$  from  $Da$  mentioned in section 4.3 by use of the velocity triangle at the outlet of the rotor blade as shown in figure 10. In figure 10,  $AE$  equals to  $AG$  and  $CD$  ( $=2 \cdot Da$ ). That is, the relationship between  $D$  and  $Da$  is given by the next equation

$$D = Da \cdot \cos \beta_2 / \cos \theta = 2Da \cos \beta_2 \quad (4)$$

where  $\beta_2$  and  $\theta$  is the relative outlet flow angle and absolute outlet flow angle respectively. From equation (4) it is definite that even if  $Da$  doesn't change,  $D$  changes by the flow angle.

Figure 11 shows the distribution of the wake width  $D$  to the radial distance at the each flow rate. At the  $\eta_{\max}$ -point ( $\circ$ ) and  $SPL_{SI}$ -point ( $\triangle$ ),  $D$  is the small value because the flow is attached to the blade surface at all radial positions. At the  $SPL_{\max}$ -point ( $\square$ ), it is characteristic that  $D$  is large in  $R > 220\text{mm}$  conspicuously, but in  $R = 200\text{mm}$ ,  $D$  is as small as that at the attached flow condition. Meanwhile, the distribution of  $D$  at  $SPL_{\min}$ -point ( $\nabla$ ) and near cut-off point ( $\diamond$ ) are resemble qualitatively.

From these characteristics it is evident that at first in  $\phi = 0.172$  the back flow occurs at the trailing edge near the blade tip and then main flow possesses radial outward flow component toward the blade trailing edge, but at the trailing edge the main flow separated over  $1/2$  blade height from the blade tip, and next in  $\phi = 0.104$  the outward flow becomes remarkable, and then the flow at the trailing edge near

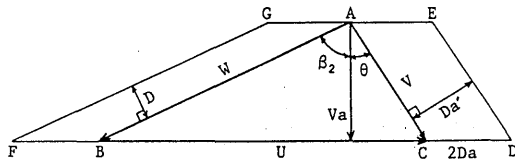


Fig. 10 Velocity triangle.

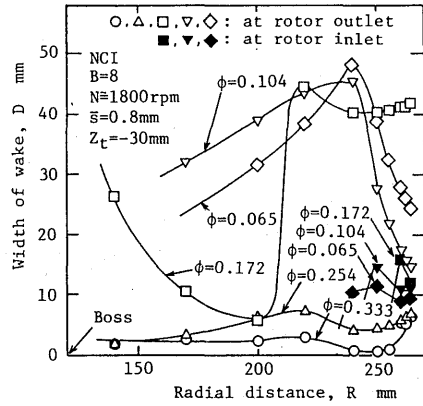


Fig. 11 Effects of flow rate on the wake width.

the blade tip increases in spite of the total flow decrease and then  $D$  becomes small for the flow attached.

When the back flow occurs, the wake arises upstream of the blade and in such circumstances its width is very small compared with one downstream of the blade, as shown with black painted symbols in figure 11.

4.5 Comparison between measured and predicted values of noise Figure 12 shows the spectral density distribution of noise for three flow rates i. e.  $\phi=0.333, 0.172, 0.104$ . In  $\eta_{max}$ -point ( $\phi=0.333$ ), the discrete peaks of sound pressure level are shown at about 235Hz, 470Hz, ..... These are the interaction noise which generated by the interaction between rotor blade and the distorted duct wall. The values  $n=1$  and 2 in this figure correspond to the fundamental tone (235Hz) and the over tone. The values of turbulent noise are estimated with subtracting the values of discrete frequency noise from over all noise. These values were compared with theoretical values. The sound pressure level of the turbulent noise obtained from a such management is equal to the level at the duct wall not distorted, i. e. the interaction noise not generated. In the  $SPL_{max}$ -point ( $\phi=0.172$ ) and  $SPL_{min}$ -point ( $\phi=0.104$ ), the discrete frequency noises are barely shown in about 150Hz and 180Hz band. These seem to be the resonant noise which generated by the resonance between rotor wake and fan duct system<sup>(8,11)</sup>. In this case, the turbulent noise is obtained by subtracting overall noise energy from discrete frequency noise. The turbulent noise is almost flat over 0.2-2kHz band in  $\phi=0.333$ , but noise energy exists mainly over 0.15-0.4kHz band in  $\phi=0.172$  and 0.104.

Well as seen from equation (1), the acoustic power  $E$  is able to estimate, if  $W$  and  $D$  are given. But at the low flow rate condition,  $W$  at the blade inlet and the wake width  $D$  aren't given at the

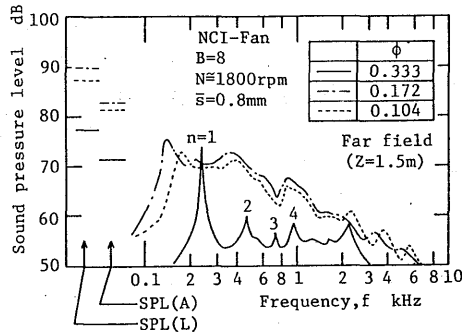


Fig. 12 Comparison of spectral density distribution.

same radial position because the main flow possesses the radial outward flow component. In this report, firstly we seek for the point A from figure 4(a) at which  $V_a=0$ , and then draw an equivalent line AC to AB which is the distance between point A and blade tip. We thought that the separation region was from tip to point C. It was assumed that the flow at point C reached point D at blade tip in trailing edge side and the fluid in smaller radial position than D flows in parallel with CD. In such way, we also estimate the sound pressure level generated from the back flow, but this value was about 7% of the values at trailing edge, therefore it can be ignored in the most case. In this report, we adopted the sum of the former and latter.

Figure 13 shows the comparison between the measured sound pressure level and the theoretical values obtained from the following method that at first the acoustic power E is calculated from equation (1) with substituting the wake width D in figure 11 and the relative velocity W in figure 7 and next the sound pressure level is calculated with substituting E for equation (2). It is shown that the calculated values well agree with measured ones quantitatively over the all flow rate in this experiment. From the above mentioned results, the change in the sound pressure level with the flow rate is closely related with the flow conditions at the vicinity of the blade tip, i.e., in the case of the magnitude of wake width in the flow region where the relative velocity is large, the sound pressure level becomes high.

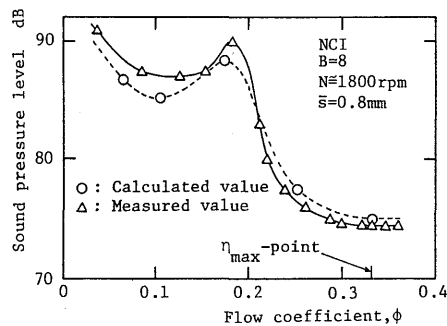


Fig. 13 Flow characteristics of sound pressure level.

## 5. Conclusion

In this investigation, we surveyed the flow rate characteristics of the sound pressure level relating to the flow condition around the rotor blades and predict the sound pressure level over whole flow region. The results are summarized as follows.

- (1) The turbulent noise generated from the fan is related to the flow condition around the rotor blade, especially, the vicinity of the blade tip. And so the wake width is larger, the sound pressure level is higher.
- (2) If the wake width and the relative velocity are given, the turbulent noise can be estimated from equation(1) and (2) over the whole flow rate containing the low flow rate region.
- (3) The flow characteristics of sound pressure level of the fan noise can be explained over wide flow rate region.

## References

- (1) Longhouse, R. E., J. Sound Vib., 48-4(1976), 461.
- (2) Kodama, Y. and Fukano, T., Trans. JSME, 52-475(1986), 1316.
- (3) Kusama, H. et al., Preprint of the JSME, No.754-3(1975), 76.

- (4) Mather, J. S. B., et al., J. Sound Vib., 16-3(1971), 407.
- (5) Senoo, Y. and Kodama, Y., Trans. JSME, 39-320(1973), 1246.
- (6) Fukano, T. et al., Trans. JSME, 51-463(1985), 820.
- (7) Fukano, T. and Kodama, Y., Trans. JSME, 51-466(1985), 1825.
- (8) Fukano, T. and Kodama, Y., Trans. JSME, 52-477(1986), 2131.
- (9) Sharland, I. J., J. Sound Vib., 1-3(1975), 302.
- (10) Fukano, T. et al., Trans. JSME, 41-245(1975), 1479.
- (11) Fukano, T. et al., Trans. JSME, 43-370(1977), 2199.